IEEE Access
Multidisciplinary | Rapid Review | Open Access Journal

Received January 8, 2020, accepted January 19, 2020, date of publication January 29, 2020, date of current version February 6, 2020.

Digital Object Identifier 10.1109/ACCESS.2020.2970158

Hybrid-Weighted Total Variation and Nonlocal Low-Rank-Based Image Compressed Sensing Reconstruction

HUI ZHAO, YANZHOU LIU, CHENG HUANG, AND TIANLONG WANG
School of Communication and Information Engineering, Chongqing University of Posts and Telecommunications, Chongqing 400065, China
Corresponding author: Hui Zhao (zhaohui@cqupt.edu.cn)

This work was supported by the National Natural Science Foundation of China (No. 61671095).

ABSTRACT To reconstruct natural images from compressed sensing (CS) measurements accurately and effectively, a CS image reconstruction algorithm based on hybrid-weighted total variation (HWTV) and nonlocal low-rank (NLR) is proposed. It considers the local smoothness and nonlocal self-similarity (NSS) in image, improves traditional hybrid total variation (TV) model, and constructs a new edge detection operator with mean curvature to adaptively select the TV. The HWTV combines the advantages of first-order TV and second-order TV to preserve the edges of the image and avoid the staircase effect in the smooth areas. And NLR can effectively reduce the redundant information and retain the structural information of the image. In addition, the proposed algorithm constructs prior regularization terms with improved HWTV model and NLR model, and utilizes soft threshold function and smooth but non-convex function to solve the TV and low-rank optimization problems, respectively. Finally, the alternative direction multiplier method (ADMM) iterative strategy is used to separate the target model into several sub-problems, and the most efficient methods are adopted to solve each sub-problem. Experimental results show that, compared with the state-of-the-art CS reconstruction algorithms, the proposed algorithm can achieve higher reconstruction quality, especially in the case of low sampling rates.

INDEX TERMS Image reconstruction, compressed sensing, hybrid-weighted total variation, nonlocal low-rank.

I. INTRODUCTION

Compressed sensing [1], [2] theory proposes a new sampling framework, which simultaneously samples and compresses sparse or compressible signals at a sampling rate significantly below Nyquist's sampling theorem [3], and can perfectly reconstruct the signal from only a small number of linear measurements by the corresponding optimization algorithm. In the theory of CS, if a signal $u \in R^n$ is sparse (or compressive), then the signal $u \in R^n$ can be perfectly reconstructed from its m randomized linear measurements $y = \Phi u + v$, $y \in R^m$, where $\Phi \in R^{m\times n}(m \ll n)$ is the observation matrix and v denotes additive Gaussian white noise vector. Observation matrix can be regarded as a degenerate operation in the process of observation, so signal reconstruction is essentially an ill-posed inverse problem. The CS theory guarantees perfect reconstruction of u if Φ satisfies the restricted isometry property (RIP). In order to obtain a more reasonable estimation with high robustness, it is usually necessary to rely on prior information of the original signal, and then the estimation of the original signal can be expressed as an optimization problem based on regularization. The general unconstrained optimization model for solving the inverse problem can be expressed as

$$\hat{u} = \arg\min_{u} \frac{1}{2} \|y - \Phi u\|_2^2 + \lambda \mathcal{R}(u), \tag{1}$$

where the first term is the data fidelity term, which measures the closeness of the estimate to the original signal. And the second term is the regularization constraint term, which represents the prior information of the original signal and is used to penalize the estimation of the expected property. λ is a regularization parameter controlling the trade-off between these two terms.

The classic smoothness prior information regularization term, such as TV regularization model [4], achieves good

The associate editor coordinating the review of this manuscript and approving it for publication was Hengyong Yu.

denoising effect while preserving image edge information, but often produces staircase effect in the image smooth areas and penalizes gradients uniformly, which can not effectively distinguish high frequency pixels such as image edge and noise. To avoid the staircase effect of the first-order TV model in the smooth areas, many studies replace the traditional TV regularization term with the higher order TV regularization term [5]-[8]. Due to the fact that the solution obtained by the second-order TV regulation term constraint is piece-wise linear, it can better describe the grayscale change of the image in smooth areas so as to avoid the staircase effect. However, the second-order TV usually blurs the edges of the original image. Therefore, many researchers have developed combining the first-order TV and higher-order TV [9], [10] to avoid the staircase effect while preserving the edge structure of the image. However, most of the traditional hybrid total variation (HTV) models do not take the structural features of the image into consideration, and can not effectively distinguish the edges, noise and smooth areas of the image, making the image reconstruction effect unsatisfactory.

Aiming at the problem that the traditional first-order TV model has the same penalty for all gradients, a weighted TV model has been proposed [11]. The core idea of the weighted strategy is to set a smaller weight for the pixels with larger gradients, which makes the model preserve the edges of the image better than the traditional TV model. However, existing weighted TV strategies generally utilize the gradient of the image to construct the weight coefficient, and can not make full use of the structural features of the image, which leads to the algorithms susceptible to noise, and easy to introduce wrong textures into reconstructed images.

In addition to smooth sparse prior, the NSS is also an important property in natural images [12]-[17], which describes the repeatability of image structures. The NSS based NLR-CS model [16] can effectively reduce the redundant information and retain the structure information of the image. However, it always destroys the key details of the image and fails to preserve edge structures.

Based on the above problems, this paper proposes a new HWTV and NLR models based image CS reconstruction algorithm. The main contributions are as follows:

(1) A new edge detection operator is constructed by the mean curvature based on the second derivative. By setting the threshold value for the edge detection operator, the first-order TV model or the second-order TV model in the HTV are selected adaptively. At the same time, the first-order TV model is weighted, and the new weight coefficient is constructed by difference curvature to improve the ability of the edge preservation and denoising performance of the algorithm.

(2) The improved HWTV model is introduced into the NLR-CS reconstruction algorithm, the proposed algorithm is the first one to combine NLR with HTV regularization in a single effective model, which effectively describes the NSS and local smoothness sparsity of natural images in a unified framework. The TV regularization term and the NLR regularization term are complementary to each other, the NSS prior is utilized to eliminate the influence of global information loss in traditional algorithms and preserve the texture and other structural information of images, the local smoothness prior is utilized to suppress noise, to reduce or remove the false information generated in the process of low rank matrix recovery and preserve edge and other complex structure information. Appropriate adjustment of the weights of these two regularization terms can achieve better reconstruction effects.

(3) In order to simplify the solving process of the algorithm model, an optimization solution based on ADMM iterative strategy is designed. The solution problem of the algorithm is separated into several sub-problems, and each sub-problem is solved efficiently.

(4) Experimental results verify the effectiveness of the proposed algorithm. The subjective visual effects, objective peak signal-to-noise ratio (PSNR) and structural similarity (SSIM) of the reconstructed image are better than thoes of the compared image CS reconstruction algorithms.

The remainder of the paper is organized as follows. Section II briefly introduces the NLR model. Section III elaborates the design of algorithm based on HWTV and NLR models, and gives the implementation details of solving optimization problem. Experimental results and analysis are reported in Section IV. In Section V, we conclude this paper.

II. NLR MODEL

The NLR-CS algorithm was proposed by Dong *et al.* [16], in which the NLR is regarded as a prior regularization term constraint. For each image exemplar patch, the NLR-CS algorithm first finds plenty of similar patches in other positions. Then the exemplar patches and the similar patches are made up of a data matrix X_i which may be corrupted by some noise. One solution is to model the data matrix X_i as X_i=$L_i + S_i$, where L_i and S_i denote the low-rank matrix and the Gaussian noise matrix, respectively. Thus the NLR-CS model can be described as

$$(u, L_i) = \arg\min_{u,L_i} \|y - \Phi u\|_2^2 + \lambda \sum_i \left\{ \|R_i u - L_i\|_2^2 + \eta rank(L_i) \right\}, \quad (2)$$

where $R_i u = [R_{i1}u, R_{i2}u, \cdots R_{ih}u]$ denotes the similar patches group matrix X_i, rank(•) is the rank function.

III. HWTV AND NLR BASED IMAGE CS RECONSTRUCTION ALGORITHM

A. HWTV MODEL

In order to enhance the adaptability and denoising performance of the traditional HTV, this section proposes a new edge detection operator for HTV model and a new weighted strategy for first-order TV.

The HTV model is generally expressed as

$$HTV(u) = \sum_i \alpha_i |Du|_i + (1 - \alpha_i) \left| D^2 u \right|_i \quad (3)$$

with

$$|Du|_i = \sqrt{(D_x u)_i^2 + (D_y u)_i^2} \tag{4}$$

and

$$\left|D^2 u\right|_i = \sqrt{(D_{xx} u)_i^2 + (D_{xy} u)_i^2 + (D_{yx} u)_i^2 + (D_{yy} u)_i^2}, \tag{5}$$

where α_i is a trade-off coefficient which generally utilizes the edge detection operator to balance the HTV. Eq.(4) and Eq.(5) are first-order TV and second-order TV, respectively. $(D_x u)_i$, $(D_y u)_i$ are the first-order difference operators of the current pixel i in the horizontal direction and the vertical direction, respectively. $(D_{xx} u)_i$, $(D_{xy} u)_i$, $(D_{yx} u)_i$, and $(D_{yy} u)_i$ are the second-order difference operators of the current pixel i in different directions. Due to the complexity of the image structure and the fact that the first-order TV model has the same penalty for all gradients of the image, the traditional edge detection operator based on image gradient can not effectively distinguish the edges, noise and smooth areas of the image.

In order to distinguish edges and smooth areas of image better, we construct a new edge detection operator of HTV by using the mean curvature M [18] and setting threshold σ. For the i-th pixel, it is defined as

$$M_i = \frac{(u_{\eta\eta})_i + (u_{\xi\xi})_i}{2} \tag{6}$$

with

$$u_{\eta\eta} = \frac{u_x^2 u_{xx} + 2u_x u_y u_{xy} + u_y^2 u_{yy}}{u_x^2 u_y^2} \tag{7}$$

and

$$u_{\xi\xi} = \frac{u_y^2 u_{xx} - 2u_x u_y u_{xy} + u_x^2 u_{yy}}{u_x^2 u_y^2}, \tag{8}$$

where u_x and u_y represent the first-order gradients of the current pixel i along x (horizontal) and y (vertical) directions, respectively. u_{xx}, u_{xy}, u_{yx} and u_{yy} represent the second-order gradients of the current pixel i. The first-order TV model can effectively preserve the edge structure of the image, and the second-order TV model can effectively remove the staircase effect in the image smooth areas. Therefore, the adaptive TV strategy is proposed in this paper. When $M_i > \sigma$, $\alpha_i = 1$ (i is the pixel position), meaning that only the first-order TV acts on edge and noise mixed areas, which can effectively preserve the edges of the image and denoising. When $M_i \leq \sigma$, $\alpha_i = 0$, meaning that only the second-order TV acts on the smooth areas, which can avoid the staircase effectively. This adaptive strategy makes full use of the characteristics of first-order TV and second-order TV, and achieves better reconstruction effect as shown in Section 4.

When the image is reconstructed by the traditional HTV model, the non-smooth areas (edges, noise) of the image are mainly dominated by the first-order TV and the effect of all pixel points in the region is consistent. On the one hand, edges of the image will be blurred when denoising, on the other hand, the effect of denoising can not be achieved when preserving the edge. According to the above problem, the first-order TV in the HTV is improved, that is, the TV is weighted, and a new HWTV model is proposed as

$$HWTV(u) = \sum_i \left\{ \alpha_i \omega_i |Du|_i + (1 - \alpha_i) \left|D^2 u\right|_i \right\}. \tag{9}$$

Here the weight factor ω_i is constructed by utilizing the indicator based on the second derivative difference curvature C [18] as

$$\omega_i = \frac{1}{C_i + \theta}, \tag{10}$$

where

$$C_i = \left| |(u_{\eta\eta})_i| - |(u_{\xi\xi})_i| \right| \tag{11}$$

and θ is a constant. For edges, $|(u_{\eta\eta})_i|$ is large and $|(u_{\xi\xi})_i|$ is small, so C_i is large. For noise, $|(u_{\eta\eta})_i|$ and $|(u_{\xi\xi})_i|$ are both large and almost equal, so C_i is small. Therefore, according to C_i, the edges and noises of the image can be distinguished effectively. The new weighted strategy not only preserves edges of the image but also improves the denoising performance of the proposed algorithm.

B. RECONSTRUCTION OPTIMIZATION MODEL

Through the above analysis and theoretical basis, the objective function of the proposed HWTV and NLR based image CS reconstruction model can be expressed as

$$\begin{aligned} \arg\min_u \frac{1}{2} \|y - \Phi u\|_2^2 \\ + \lambda_1 \sum_i \left\{ \alpha_i \omega_i |Du|_i + (1 - \alpha_i) \left|D^2 u\right|_i \right\} \\ + \lambda_2 \sum_i \left\{ \|R_i u - L_i\|_2^2 + \eta rank(L_i) \right\}, \end{aligned} \tag{12}$$

where λ_1, λ_2, and η are trade-off parameters. The first term of Eq.(12) is the data fidelity term, the second term is the HWTV regularization term, and the third term is the NLR-CS regularization term. Since Eq.(12) contains low-rank matrix minimization and different gradient optimization problems, the direct solving is very complicated. In order to simplify the solving process of the proposed algorithm model, we utilize the ADMM [19] method framework to optimize the proposed objective function. The solving process of the proposed algorithm is as follows.

First, we rewrite Eq.(12) into a constrained one by introducing auxiliary variable x, z_1, z_2, and utilize iterative optimization strategy to solve it. One of the advantages of this transformation is that the problem can be simplified further by splitting it into sub-problems which are easier to solve. The constrained model is

$$\begin{aligned} \arg\min_{u, L_i, x, z_1, z_2} \frac{1}{2} \|y - \Phi u\|_2^2 \\ + \lambda_1 \sum_i \left\{ \alpha_i \omega_i |z_1|_i + (1 - \alpha_i) |z_2|_i \right\} \end{aligned}$$

$$+\lambda_2 \sum_i \left\{ \|R_i x - L_i\|_2^2 + \eta rank(L_i) \right\}$$
$$s.t.\ u = x, Du = z_1, D^2 u = z_2. \tag{13}$$

Thus, the corresponding augmented Lagrangian function of Eq.(13) is given by

$$\begin{aligned} \arg\min_{u,L_i,x,z_1,z_2} & \frac{1}{2}\|y - \Phi u\|_2^2 \\ & + \lambda_1 \sum_i \{\alpha_i \omega_i |z_1|_i + (1-\alpha_i)|z_2|_i\} \\ & + \lambda_2 \sum \left\{ \|R_i x - L_i\|_2^2 + \eta rank(L_i) \right\} \\ & + \frac{\mu_1}{2}\|x - u + a\|_2^2 + \frac{\mu_2}{2}\|z_1 - Du + b\|_2^2 \\ & + \frac{\mu_3}{2}\left\| z_2 - D^2 u + c \right\|_2^2, \end{aligned} \tag{14}$$

where μ_1, μ_2, μ_3 are penalty parameters, and a, b, c are Lagrangian multipliers. The ADMM method can be regarded as the original dual method of finding the saddle point problem (augmented Lagrangian). Therefore, the saddle point of Eq.(14) is the optimal solution of the original problem Eq.(12).

Then, we decompose Eq.(14) into four simpler minimization sub-problems (a)-(d) to obtain the solution.

Sub-problem (*a*)**:** The z_1 and z_2 sub-problems are given as

$$\begin{aligned} z_1^{k+1} = & \arg\min_{z_1} \lambda_1 \sum_i \alpha_i \omega_i |z_1|_i \\ & + \frac{\mu_2}{2}\left\| z_1 - Du^k + b^k \right\|_2^2 \end{aligned} \tag{15}$$

and

$$\begin{aligned} z_2^{k+1} = & \arg\min_{z_2} \lambda_1 \sum_i (1-\alpha_i)|z_2|_i \\ & + \frac{\mu_3}{2}\left\| z_2 - D^2 u^k + c^k \right\|_2^2, \end{aligned} \tag{16}$$

which can be solved by the shrinkage operator [20] as

$$\begin{aligned} (z_1)_i^{k+1} = & \max\left\{ |Du - b|_i - \frac{\lambda_1 \alpha_i \omega_i}{\mu_2}, 0 \right\} \\ & \circ \mathrm{sign}(Du - b)_i \end{aligned} \tag{17}$$

and

$$\begin{aligned} (z_2)_i^{k+1} = & \max\left\{ \left| D^2 u - c \right|_i - \frac{\lambda_1(1-\alpha_i)}{\mu_3} I_i, 0 \right\} \\ & \circ \mathrm{sign}(D^2 u - c)_i. \end{aligned} \tag{18}$$

Here I is the identity matrix, $\mathrm{sign}(x)$ is a signum function, when x is greater than or equal to 0, it is 1, and when x is less than 0, it is -1, $\circ$ is equivalent to a multiplication.

Sub-problem (*b*)**:** The L_i sub-problem is given as

$$L_i^{k+1} = \arg\min_{L_i} \sum_i \left\{ \left\| R_i x^k - L_i \right\|_2^2 + \eta rank(L_i) \right\} \tag{19}$$

Since the low-rank solution of matrix is a NP-hard problem, which can not be solved directly. Dong et.al. utilize smooth but non-convex function $L(L_i, \varepsilon)$ to approximate $rank(L_i)$, and point out that the low-rank approximate effect of $\log\det(\cdot)$ is better than the nuclear norm $\|\cdot\|_*$ (sum of the singular values). Here, we replace $rank(L_i)$ with $L(L_i, \varepsilon)$, which is a $\log\det(\cdot)$ surrogate function and can be defined as

$$L(L_i, \varepsilon) = \log\det((L_i L_i^T)^{1/2} + \gamma I), \tag{20}$$

where γ is a positive constant and I denotes the identity matrix. The iterative process is as follows

$$L_i^{k+1} = U(\widetilde{\Sigma} - \tau diag(\xi_j^{(k)}))_+ V^T, \tag{21}$$

where $U \widetilde{\Sigma} V^T$ is SVD (Singular Value Decomposition) of X_i, $\tau = \eta/2\lambda_2$, $(x)_+ = \max(x, 0)$, and $\xi_j^{(k)} = 1/(\sigma_j^{(k)} + \varepsilon)$, σ_j is the j-th singular value of L_i.

Sub-problem (*c*)**:** The x sub-problem is

$$x^{k+1} = \arg\min_x \lambda_2 \sum_i \|R_i x - L_i\|_2^2 + \frac{\mu_1}{2}\left\| x - u^k + a^k \right\|_2^2. \tag{22}$$

The x sub-problem essentially is minimization problem of strictly convex quadratic function. Setting the gradient of x^{k+1} to be zero gives a closed solution for Eq.(22), which can be expressed as

$$x^{k+1} = \frac{\lambda_2 \sum_i R_i^T L_i + \mu_1(u^k - a^k)}{\lambda_2 \sum_i R_i^T R_i + \mu_1 I}, \tag{23}$$

where I is an identity matrix. $\sum_i R_i^T R_i$ is a diagonal matrix. Each element in the diagonal matrix corresponds to the image pixel position, the value of the element is the number of overlapping patches that cover the pixel location. $\sum_i R_i^T L_i$ denotes the patches average result-i.e., averaging all of the collected similar patches for each exemplar patch [16].

Sub-problem (*d*)**:** The u sub-problem is

$$\begin{aligned} u^{k+1} = & \arg\min_u \frac{1}{2}\|y - \Phi u\|_2^2 + \frac{\mu_1}{2}\left\| x^k - u + a^k \right\| \\ & + \frac{\mu_2}{2}\left\| {z_1}^k - Du + b^k \right\|_2^2 + \frac{\mu_3}{2}\left\| {z_2}^k - D^2 u + c^k \right\|_2^2, \end{aligned} \tag{24}$$

which also has a closed form solution as

$$u^{k+1} = \frac{\begin{pmatrix} \Phi^T y + \mu_1(x^k + a^k) \\ + \mu_2 D^T({z_1}^k + b^k) + \mu_3 (D^2)^T({z_2}^k + c^k) \end{pmatrix}}{\Phi^T \Phi + \mu_1 I + \mu_2 D^T D + \mu_3 (D^2)^T D^2}. \tag{25}$$

Eq.(25) can be solved effectively by the preconditioned conjugate gradient (PCG) method [12].

Now, after solving the above four sub-problems, the multipliers can be updated as

$$\begin{cases} a^{k+1} = a^k - (u^{k+1} - x^{k+1}) \\ b^{k+1} = b^k - (Du^{k+1} - {z_1}^{k+1}) \\ c^{k+1} = c^k - (D^2 u^{k+1} - {z_2}^{k+1}), \end{cases} \tag{26}$$

and next iteration is performed until the iteration termination condition is satisfied. The output u^{k+1} of the last iteration is the reconstructed image $\widetilde{u}$ of the original image.

The complete algorithm procedure can be summarized as algorithm 1.

Algorithm 1 HWTV and NLR Based Image CS Reconstruction Algorithm

Input: $y, u_0 = \Phi^T y, a, b, c, \lambda_1, \lambda_2, \mu_1, \mu_2, \mu_3, M_i$.
Out loop: for $k = 1, 2, \cdots, K$
Find the position of similar pixels in the image based on the patch matching method
if $k \leq K_0 \omega_i = 1$ **else** Calculated ω_i by Eq.(10).
Inner loop for $t = 1, 2, \cdots, T$
Update ${z_1}^{k+1}$ and ${z_2}^{k+1}$ by Eq.(17) and Eq.(18), respectively.
Update ${L_i}^{k+1}$ and x^{k+1} by Eq.(21) and Eq.(23), respectively.
Update u^{k+1} by Eq.(25).
Update ${M_i}^{k+1}$ by Eq.(6).
End for
Update a, b, and c by Eq.(26).
End for
return: the reconstruction image $\widetilde{u} = u^{k+1}$.

IV. SIMULATION RESULTS

In this part, we compare our proposed algorithm with the classical GSR-NCR algorithm [13], NLR-CS algorithm [16], and TVNLR algorithm [17] by simulation results. The performance evaluation indexes are PSNR (dB), SSIM and Time(s). Six natural grayscale images of 256 × 256 are selected as test images, which are Barbara, Boats, Cameraman, Lena, Monarch and Parrots. The observation matrix Φ is a random observation matrix. M is initialized to identity matrices. According to [17], K, T, K_0 are set to 18, 15, and 5, respectively. The sampling rate is set from 0.01 to 0.30. For example, when the sampling rate is 0.05, the original image information obtained is less, but the original image can be reconstructed with high quality from less information, which fully demonstrates that the reconstruction algorithm has superior performance. For better CS recovery performation, the regularization parameters λ_1 and λ_2 are tuned separately according to each sub-rate, so are the Lagrangian multipliers a, b, and c. As shown in Subsection A to Subsection D, empirically, the number of iterations is set to 270, the number of similar patches is 45, the size of the matching window of the similar patches is 20 × 20 image areas which is centered on the current exemplary patch, and the size of the exemplary patches is set to 6 × 6. All the simulations are performed in Matlab 2016a environment on a PC with Intel(R) Core(TM) i5-8500 CPU @3.30GHz, 8G ARM, and Windows 10 operating system.

A. ALGORITHM STABILITY

Since the objective function (13) is non-convex, it is difficult to prove its global convergence theoretically. Here, we provide empirical evidence to illustrate the stability of the proposed algorithm. Fig.1 (a) and Fig.1 (b) show the PSNR iterative curves of test images Boats, Cameraman, Lena, and Monarch when the sampling rates are 0.05 and 0.20, respectively. It can be observed that with the increase of iteration number, the PSNR curves increase monotonically and ultimately become flat and stable when iteration number over 270, which fully proves good stability of the proposed algorithm. Therefore, we empirically sets the total iteration numbers of all algorithms to 270.

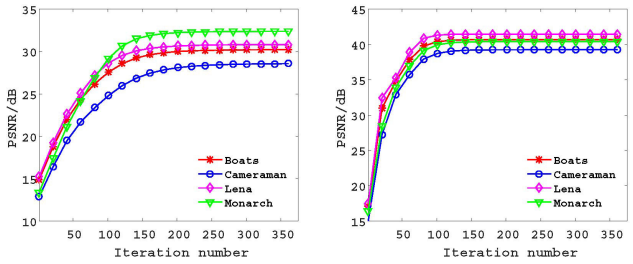

FIGURE 1. Stability analysis of the proposed algorithm. (a) The PSNR results in the case of sampling rate with 0.05; (b) The PSNR results in the case of sampling rate with 0.20.

B. EFFECT OF NUMBER OF SIMILAR PATCHES

The number of similar patches refers to the maximum number of image similar patches allowed in the process of constructing low-rank matrices. The core idea of NLR model is to solve the rank minimizing problem of low-rank matrix constructed by exemplar patches and its similar patches. The measure of similar patches is not the absolute similarity between image structure and content, but the Euclidean distance. On the one hand, if the number of image similar patches is too large, in fact, it is impossible to find enough similar patches to destroy the key details of the image. On the other hand, if the number of similar patches is too small, the details such as image edge and texture can not be completely reconstructed. Therefore, in order to verify the influence of image similar patches number on the proposed algorithm, we vary the similar patches number from 40 to 65. The experimental results are shown in Fig.2 (a) and Fig.2 (b). It can be seen that the performance of the algorithm may decline with the increase of image similar patches number. Based on the comprehensive considerations, the algorithm performs best when the number of similar patches is 45. For this reason, this paper sets the number of similar patches to 45 empirically.

C. EFFECT OF SIMILAR PATCH MATCHING WINDOW SIZE

In this subsection, we will give the detailed description about how to select the best matching window size, which makes the proposed algorithm achieving the best reconstruction effect.

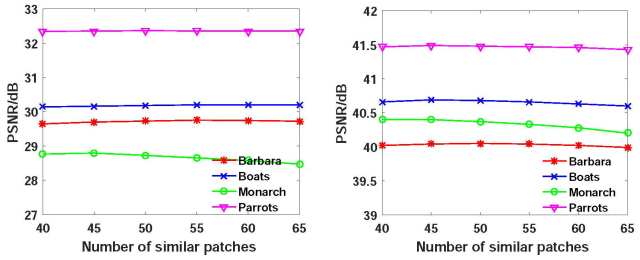

FIGURE 2. Effect of number of similar patches. (a) Simulation results in the case of sampling rate with 0.05; (b) Simulation results in the case of sampling rate with 0.20.

TABLE 1. Effect of similar patch matching window size on reconstruction performance.

Iamge	Sampling rate	Index	15×15	20×20	30×30	45×45
Barbara	0.20	PSNR/dB	40.06	40.04	39.98	39.91
	0.30	PSNR/dB	43.09	43.10	43.08	43.04
Boats	0.20	PSNR/dB	40.67	40.69	40.66	40.61
	0.30	PSNR/dB	43.91	43.90	43.90	43.85
Cameraman	0.20	PSNR/dB	39.16	39.24	39.27	39.23
	0.30	PSNR/dB	43.78	43.83	43.82	43.82

To reduce the computational complexity in the construction of low-rank matrix, the similar image patches are searched in a certain region centered on the current image patches, which effectively avoids the high computational complexity caused by the global search for image similar patches. Specifically, in order to study the sensitivity of matching windows size to the proposed algorithm, four matching windows of different sizes are set up by simulation with several test images at sampling rates of 0.20 and 0.30. As can be seen from Table 1, when the search window size is different, the performance of CS image reconstruction remains stable basically. Based on the computational complexity and performance, this paper sets the similar patch matching window size to 20 empirically.

D. EFFECT OF OVERLAPPING PATCH SPACING

The overlapping exemplar image patch spacing refers to the distance between two connected exemplar patches in the process of dividing the image into overlapping exemplar image patch, which is usually based on pixel. The size of the exemplar image patch used in this paper is. When the spacing between the connected exemplar image patches is one pixel, it means that there is only one row or one column difference between the connected exemplar image patch. When the spacing between the connected exemplar image patches is 6 pixels, it means that all exemplar image patches do not overlap each other. If the spacing between overlapping patches is too small, the number of exemplar image patches is too large and the computational complexity increases. If the spacing between overlapping patches is too large, the redundant information between overlapping patches can not be fully utilized, and the global structure information of the image can not be effectively recovered.

TABLE 2. Effect of overlapping exemplar image patch spacing on reconstruction performance.

Iamge	Index	1	2	3	4	5	6
Lena	PSNR/dB	41.51	41.51	41.51	41.48	41.46	41.35
	Time/s	2097.95	547.24	264.50	166.118	113.66	97.60
Monarch	PSNR/dB	40.48	40.48	40.45	40.45	40.40	40.25
	Time/s	2094.05	550.46	267.45	168.82	115.84	98.47
Parrots	PSNR/dB	41.55	41.55	41.54	41.52	41.49	41.43
	Time/s	2088.72	550.37	265.68	167.10	114.05	97.82

In order to verify the effect of overlapping exemplar image patch spacing for the proposed algorithm, this paper gives the performance comparison of different overlapping patches spacing in test images Lena, Monarch, Parrots with sampling rate of 0.20. The performance evaluation indexes are PSNR and CPU running time. As shown in Table 2, the smaller the overlapping patch spacing is, the greater the computational time is, and the difference of overlapping exemplar image patch spacing has little effect on the PSNR value. Based on computational complexity and performance, the best performance is usually between 4 pixels and 5 pixels, so we extract exemplar image patch in every 5 pixels along both horizontal and vertical directions empirically.

E. SIMULATIONS ON NOISELESS IMAGE

In the noiseless condition, the reconstruction quality of three algorithms is compared with different sampling rates. Fig.3, Fig.4 and Fig.5 show the reconstructed results of the test images Barbara, Cameraman and Monarch with sampling rate 0.05, respectively. It can be seen that the GSR-NCR and TVNLR algorithms have the worst reconstruction performance and the structural loss of the edge and detail of the image, the GSR-NCR algorithm is particularly obvious. The NLR-CS algorithm utilizes the NSS of the image and reconstructs original image by low-rank optimization, which preserves the overall structural features of the image to a certain extent, and can reconstruct the general outline of the image relatively clearly. However, structural information such as edges and details of the image cannot be effectively recovered, and the block effect (the so-called staircase effect) can be seen clearly. In compared, the algorithm proposed in this paper achieves the optimal subjective visual effect. The proposed algorithm takes into account the NSS and local smooth sparsity of the image, effectively makes up the shortcomings of the NLR-CS model, which not only effectively preserves the edges, but avoids the staircase effect in smooth areas. The proposed algorithm makes full use of the advantages of the first-order TV preserving edge and the second-order TV preventing the staircase effect. The reconstructed image is closer to the original image. In Fig.3, the PSNR values of the proposed algorithm is increased by **10.05dB**, **7.06dB**, and **1.76dB** compared with the GSR-NCR, TVNLR and NLR algorithms, respectively. Magnified image details show that the proposed algorithm can not only perfectly reconstruct large-scale sharp edges but also well recover small-scale fine structures. It is effectively verified

FIGURE 3. CS recovered Barbara images. (a) Original image; (b) Recovered image by GSR-NCR algorithm (19.65dB); (c) Recovered image by TVNLR algorithm (22.64dB); (d) Recovered image by NLR-CS algorithm (27.94dB); (e) Recovered image by the proposed algorithm (29.70dB).

FIGURE 4. CS recovered Cameraman images. (a) Original image; (b) Recovered image by GSR-NCR algorithm (19.04dB); (c) Recovered image by TVNLR algorithm (24.39dB); (d) Recovered image by NLR-CS algorithm (25.38dB); (e) Recovered image by the proposed algorithm (28.41dB).

FIGURE 5. CS recovered Monarch images. (a) Original image; (b) Recovered image by GSR-NCR algorithm (19.31dB); (c) Recovered image by TVNLR algorithm (23.01dB); (d) Recovered image by NLR-CS algorithm(26.38dB); (e) Recovered image by the proposed algorithm (28.79dB).

that the proposed algorithm has better performance than the reconstruction algorithm which only uses a single prior information of the image.

To facilitate the evaluation of objective qualities, next, we change the sampling rate and perform simulations on different CS algorithms for all test images. Table 3 shows the PSNR and SSIM results of the reconstructed images at sampling rates between 0.01 and 0.05. Fig.6 (a) and Fig.6 (b) show average PSNR comparison for all test images at sampling rates from 0.01 to 0.05 and from 0.05 to 0.30, respectively. As can be seen from Table 3, the PSNR and SSIM gains of the proposed method are significantly higher than those of the compared algorithms at low sampling rates. For the Cameraman image, the PSNR improvement over NLR-CS, TVNLR, and GSR-NCR algorithms are approximately **3.03 dB**, **4.02 dB**, and **9.37dB** when the sampling rate is 0.05, respectively. And Fig.6 shows that, on average PSNR values, the proposed method is superior to the compared methods. As the sampling rate increases, the reconstruction quality gap between the proposed method and NLR-CS method are smaller, but it still superior to the TVNLR algorithm and GSR-NCR algorithm. Based on Table 3 and Fig.6, when the sampling rate is low and the observation value is less, the proposed algorithm can obtain better reconstruction performance and better reconstruction visual effect.

F. SIMULATION ON NOISY IMAGE

In this subsection, a similar simulation was performed to verify the robustness of the proposed algorithm to noise. A significant amount of additive Gaussian noise is added to CS measurements. The standard derivations of additive noise vary to generate the signal-to-noise ratio(SNR) between 15dB and 35dB. Fig.7 shows the PSNR values of testing images Barbara and Cameraman with sampling rate 0.05 at different noise levels, respectively. Table 4 shows the PSNR with different sampling rates and constant noise level.

TABLE 3. The PSNR and SSIM values of recovery algorithms at different sampling rates.

Iamge	Algorithm	Index	Sampling rate 0.01	0.02	0.03	0.04	0.05
Barbara	TVNLR	PSNR/dB	18.87	21.12	21.82	22.23	22.64
		SSIM	0.400	0.491	0.523	0.545	0.568
	NLR-CS	PSNR/dB	17.83	19.86	22.70	25.06	27.94
		SSIM	0.396	0.418	0.627	0.726	0.829
	GSR-NCR	PSNR/dB	16.53	18.10	18.89	19.16	19.65
		SSIM	0.378	0.431	0.500	0.513	0.547
	Proposed	PSNR/dB	**19.26**	**22.30**	**24.95**	**27.32**	**29.70**
		SSIM	**0.419**	**0.576**	**0.700**	**0.803**	**0.874**
Boats	TVNLR	PSNR/dB	19.81	21.62	22.99	23.98	24.79
		SSIM	0.501	0.567	0.627	0.665	0.696
	NLR-CS	PSNR/dB	18.62	20.69	23.67	27.58	29.80
		SSIM	0.458	0.557	0.672	0.793	0.848
	GSR-NCR	PSNR/dB	16.89	17.31	20.08	20.60	22.03
		SSIM	0.395	0.414	0.539	0.563	0.630
	Proposed	PSNR/dB	**19.99**	**23.82**	**26.67**	**28.88**	**29.70**
		SSIM	**0.497**	**0.663**	**0.765**	**0.827**	**0.856**
Cameraman	TVNLR	PSNR/dB	17.51	21.33	22.52	23.44	24.39
		SSIM	0.412	0.612	0.680	0.706	0.737
	NLR-CS	PSNR/dB	15.91	18.49	20.80	23.16	25.38
		SSIM	0.401	0.554	0.635	0.711	0.770
	GSR-NCR	PSNR/dB	16.13	17.18	17.77	18.65	19.04
		SSIM	0.484	0.505	0.549	0.582	0.596
	Proposed	PSNR/dB	**17.31**	**21.55**	**24.87**	**27.17**	**28.41**
		SSIM	**0.420**	**0.613**	**0.745**	**0.800**	**0.823**
Lena	TVNLR	PSNR/dB	19.87	22.06	23.48	24.50	25.40
		SSIM	0.562	0.634	0.683	0.716	0.745
	NLR-CS	PSNR/dB	18.98	23.43	25.95	28.70	30.64
		SSIM	0.546	0.701	0.773	0.837	0.875
	GSR-NCR	PSNR/dB	17.56	19.53	20.31	21.61	23.41
		SSIM	0.461	0.556	0.600	0.601	0.743
	Proposed	PSNR/dB	**20.77**	**24.98**	**27.79**	**29.50**	**30.79**
		SSIM	**0.572**	**0.576**	**0.815**	**0.852**	**0.878**
Manorch	TVNLR	PSNR/dB	16.55	18.69	20.41	21.78	23.01
		SSIM	0.418	0.564	0.649	0.704	0.751
	NLR-CS	PSNR/dB	15.89	17.91	20.64	23.20	26.38
		SSIM	0.452	0.552	0.677	0.761	0.843
	GSR-NCR	PSNR/dB	13.46	15.40	15.71	17.79	19.31
		SSIM	0.307	0.421	0.425	0.552	0.638
	Proposed	PSNR/dB	**17.10**	**20.67**	**23.94**	**26.84**	**28.79**
		SSIM	**0.456**	**0.640**	**0.771**	**0.852**	**0.892**
Parrots	TVNLR	PSNR/dB	**20.52**	22.35	23.69	24.81	25.90
		SSIM	**0.666**	0.712	0.749	0.776	0.799
	NLR-CS	PSNR/dB	17.03	20.69	23.98	27.74	31.71
		SSIM	0.570	0.689	0.780	0.843	0.885
	GSR-NCR	PSNR/dB	17.83	18.64	20.02	20.34	22.02
		SSIM	0.626	0.648	0.749	0.762	0.795
	Proposed	PSNR/dB	19.24	**25.37**	**29.53**	**31.26**	**32.35**
		SSIM	0.547	**0.772**	**0.855**	**0.876**	**0.890**

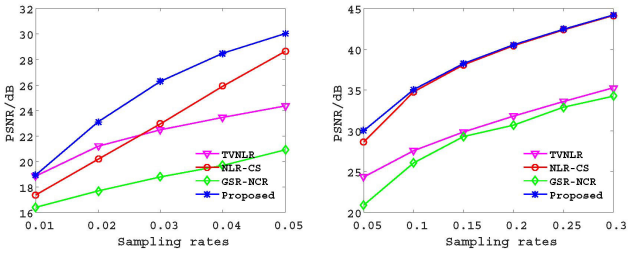

FIGURE 6. Average PSNR results of all test images. (a) Sampling rates between 0.01 and 0.05; (b) Sampling rates between 0.05 and 0.3.

One can observe from Fig.7 that the PSNR results of the proposed algorithm outperform those of the compared algorithms at different noise levels. Compared with the NLR-CS algorithm, the PSNR gains up to **3.38dB** and **3.39dB** on reconstructed images Barbara and Cameraman, respectively. As can be seen from Table 4, when the noise level is constant

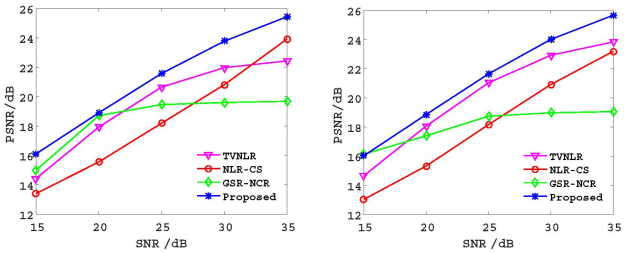

FIGURE 7. The PSNR values of the reconstructed images at different SNR. (a) Barbara test image noise measurement with sampling rate 0.05. (b) Cameraman test image noise measurement with sampling rate 0.05.

TABLE 4. The PSNR values of recovery images at different sampling rates.

SNR	Iamge	Algorithm	Sampling rate 0.05	0.10	0.15	0.20	0.25	0.30
30	Barbara	TVNLR	21.97	23.60	25.16	26.72	28.30	29.92
		NLR-CS	20.81	25.90	28.09	29.50	30.56	31.87
		GSR-NCR	19.68	**28.34**	**31.63**	**33.08**	**34.49**	**35.43**
		Proposed	**23.78**	27.55	29.65	30.96	31.78	32.49
	Cameraman	TVNLR	22.93	26.13	28.19	29.94	31.49	32.31
		NLR-CS	20.92	25.60	27.27	28.30	30.01	31.86
		GSR-NCR	19.05	22.52	25.31	26.28	28.07	29.17
		Proposed	**24.02**	**27.30**	**29.13**	**30.56**	**31.66**	**32.46**
	Manorch	TVNLR	21.98	25.86	28.31	30.29	31.94	32.65
		NLR-CS	21.33	26.43	28.33	29.66	30.95	32.34
		GSR-NCR	19.25	24.15	28.02	29.36	**32.55**	**33.99**
		Proposed	**23.82**	**27.68**	**29.80**	**31.22**	32.28	33.05

TABLE 5. Average CPU time for reconstruction images at different sampling rates.

Algorithm	Index	Sampling rate 0.05	0.10	0.15	0.20	0.25	0.30
TVNLR	Time/s	82.34	78.75	76.45	74.66	73.05	71.57
NLR-CS	Time/s	104.98	103.73	104.28	103.84	104.29	104.75
GSR-NCR	Time/s	99.25	99.12	98.85	99.12	98.74	98.39
Proposed	Time/s	**119.48**	**118.23**	**116.11**	**114.93**	**114.26**	**114.83**

(SNR is 30), PSNR values of the proposed algorithm are higher than those of the compared algorithms at different sampling rates, especially at low sampling rates.

G. ALGORITHM COMPLEXITY

To judge the complexity of the proposed algorithm intuitively, the complexity of each algorithm can be simulated theoretically by the actual running time of the algorithm. As shown in the table 5, the average CPU running time of reconstructing six images under different sampling rates are listed. From the table, we can see that the proposed algorithm is the slowest, and average CPU running time is the longest. Compared with other algorithms, the proposed algorithm has better reconstruction performance, but increases the complexity of the algorithm model. In order to reduce the CPU running time of the algorithm, one feasible method is to adopt parallelization technology.

V. CONCLUSION

The traditional CS image reconstruction algorithm only considers the single property of the image, which makes the reconstructed image less effect and the adaptability of the

algorithm is weak. In view of the above considerations, a HWTV and NLR based reconstruction algorithm is proposed in this paper. Firstly, the traditional HTV model is improved, and a new edge detection operator is constructed by utilizing the average curvature, and the TV model is selected adaptively by setting the threshold. At the same time, the weight is set for the first-order TV model, and the weight coefficient is constructed by utilizing the difference curvature. Secondly, the NSS and local smoothing sparsity are applied to a unified framework, that is, the HWTV model and the NLR-CS model are combined to construct the regularization constraints of the optimization algorithm model. Thus, it can preserve sharp edges while maintaining the smoothness in the smooth areas, and improve denoising performance. Finally, the proposed optimization algorithm model is solved by ADMM method. Extensive numerical results demonstrate the superiority of the proposed algorithm in terms of visual quality and quantitative indexes.

REFERENCES

[1] D. L. Donoho, "Compressed sensing," *IEEE Trans. Inf. Theory*, vol. 52, no. 4, pp. 1289–1306, Apr. 2006.
[2] E. Candes, J. Romberg, and T. Tao, "Robust uncertainty principles: Exact signal reconstruction from highly incomplete frequency information," *IEEE Trans. Inf. Theory*, vol. 52, no. 2, pp. 489–509, Feb. 2006.
[3] M. Unser, "Sampling-50 years after Shannon," *Proc. IEEE*, vol. 88, no. 4, pp. 569–587, Apr. 2000.
[4] L. I. Rudin, S. Osher, and E. Fatemi, "Nonlinear total variation based noise removal algorithms," *Phys. D, Nonlinear Phenomena*, vol. 60, nos. 1–4, pp. 259–268, Nov. 1992.
[5] T. Chan, A. Marquina, and P. Mulet, "High-order total variation-based image restoration," *SIAM J. Sci. Comput.*, vol. 22, no. 2, pp. 503–516, Jan. 2000.
[6] M. Lysaker, A. Lundervold, and X.-C. Tai, "Noise removal using fourth-order partial differential equation with applications to medical magnetic resonance images in space and time," *IEEE Trans. Image Process.*, vol. 12, no. 12, pp. 1579–1590, Dec. 2003.
[7] M. Bačák, R. Bergmann, G. Steidl, and A. Weinmann, "A second order nonsmooth variational model for restoring manifold-valued images," *SIAM J. Sci Comput.*, vol. 38, no. 1, pp. A567–A597, 2016.
[8] G. Liu, T.-Z. Huang, and J. Liu, "High-order TVL1-based images restoration and spatially adapted regularization parameter selection," *Comput. Math. Appl.*, vol. 67, no. 10, pp. 2015–2026, Jun. 2014.
[9] K. Papafitsoros and C. B. SchÖnlieb, "A combined first and second order variational approach for image reconstruction," *J. Math. Imag. Vis.*, vol. 48, no. 2, pp. 308–338, Feb. 2014.
[10] J.-H. Yang, X.-L. Zhao, J.-J. Mei, S. Wang, T.-H. Ma, and T.-Z. Huang, "Total variation and high-order total variation adaptive model for restoring blurred images with Cauchy noise," *Comput. Math. Appl.*, vol. 77, no. 5, pp. 1255–1272, Mar. 2019.
[11] T. Wang, K. Nakamoto, H. Zhang, and H. Liu, "Reweighted anisotropic total variation minimization for limited-angle CT reconstruction," *IEEE Trans. Nucl. Sci.*, vol. 64, no. 10, pp. 2742–2760, Oct. 2017.
[12] K. Chang, P. L. K. Ding, and B. Li, "Single image super-resolution using collaborative representation and non-local self-similarity," *Signal Process.*, vol. 149, pp. 49–61, Aug. 2018.
[13] Z. Zha, X. Zhang, Q. Wang, L. Tang, and X. Liu, "Group-based sparse representation for image compressive sensing reconstruction with non-convex regularization," *Neurocomputing*, vol. 296, pp. 55–63, Jun. 2018.
[14] R. Xiong, H. Liu, X. Zhang, J. Zhang, S. Ma, F. Wu, and W. Gao, "Image denoising via bandwise adaptive modeling and regularization exploiting nonlocal similarity," *IEEE Trans. Image Process.*, vol. 25, no. 12, pp. 5793–5805, Dec. 2016.
[15] H. Chen, X. He, L. Qing, and Q. Teng, "Single image super-resolution via adaptive transform-based nonlocal self-similarity modeling and learning-based gradient regularization," *IEEE Trans. Multimedia*, vol. 19, no. 8, pp. 1702–1717, Aug. 2017.
[16] W. Dong, G. Shi, X. Li, Y. Ma, and F. Huang, "Compressive sensing via nonlocal low-rank regularization," *IEEE Trans. Image Process.*, vol. 23, no. 8, pp. 3618–3632, Aug. 2014.
[17] J. Zhang, S. Liu, R. Xiong, S. Ma, and D. Zhao, "Improved total variation based image compressive sensing recovery by nonlocal regularization," in *Proc. IEEE Int. Symp. Circuits Syst. (ISCAS)*, May 2013, pp. 2836–2839.
[18] Q. Chen, P. Montesinos, Q. S. Sun, P. A. Heng, and D. S. Xia, "Adaptive total variation denoising based on difference curvature," *Image Vis. Comput.*, vol. 28, no. 3, pp. 298–306, Mar. 2010.
[19] C. Chen, M. K. Ng, and X.-L. Zhao, "Alternating direction method of multipliers for nonlinear image restoration problems," *IEEE Trans. Image Process.*, vol. 24, no. 1, pp. 33–43, Jan. 2015.
[20] Y. Liu, Z. Zhan, J.-F. Cai, D. Guo, Z. Chen, and X. Qu, "Projected iterative soft-thresholding algorithm for tight frames in compressed sensing magnetic resonance imaging," *IEEE Trans. Med. Imag.*, vol. 35, no. 9, pp. 2130–2140, Sep. 2016.

HUI ZHAO was born in 1980. She received the M.S. degree in fundamental mathematics and the Ph.D. degree in electronic science and technology from the Harbin Institute of Technology, China, in 2006 and 2010, respectively. She is currently a Professor with the School of Communication and Information Engineering, Chongqing University of Posts and Telecommunications. Her research interests include signal and information processing, digital communications, and wireless networks.

YANZHOU LIU is currently a Research Staff Member with the Chongqing Key Laboratory of Signal and Information Processing, Chongqing University of Posts and Telecommunications, China. His research interests include compressed sensing, signal and information processing, and image processing.

CHENG HUANG is currently a Research Staff Member with the Chongqing Key Laboratory of Signal and Information Processing, Chongqing University of Posts and Telecommunications, China. His research interests include compressed sensing, image reconstruction, and signal and information processing.

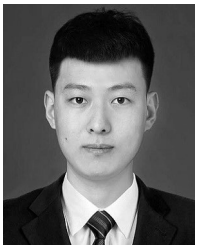

TIANLONG WANG is currently a Research Staff Member with the Chongqing Key Laboratory of Signal and Information Processing, Chongqing University of Posts and Telecommunications, China. His research interests include pattern recognition, multiobjective evolutionary algorithm, and machine learning.